THE OXIDATION PROPERTIES OF A ZIRCONIUM 2.7 w/o NIOBIUM ALLOY IN THE TEMPERATURE RANGE 300°-500°C

M.G. Cowgill, et al

McMaster University
Hamilton, Canada

June 1967

The Oxidation Properties of a Zirconium-2.7 w/o Niobium Alloy in the Temperature Range 300°-500°C

M. G. Cowgill and W. W. Smeltzer

Department of Metallurgy and Materials Science, McMaster University, Hamilton, Ontario, Canada

ABSTRACT

The reaction kinetics and structures of the alloy/oxide composite system were determined for martensitic and several Widmanstatten-structured alloys oxidized at 300°, 400°, and 500°C in oxygen at 1 atm pressure. At 300° and 400°C, there was little difference between the oxidation rates of the differently structured alloys in the early stages of the reaction. Prolonged exposures illustrated the occurrence of two limiting oxidation curves: martensitic specimens oxidized most rapidly, the oxidation rate decreasing until a transition range was attained in which the rate subsequently increased to a maximum value associated with linear kinetics; on the other hand, Widmanstatten-structured specimens containing equilibrium amounts of proeutectoid alpha-zirconium from the quench temperature oxidized most slowly, the initial decreasing oxidation rates finally approximating to linear kinetics at long exposures. Specimens containing intermediate amounts of proeutectoid alpha-zirconium oxidized at rates between these two limiting cases. At 500°C, the initial oxidation rates for all alloys approximated to parabolic kinetics, the reaction rate constants being directly dependent on the volume fractions of martensite. The oxide was cracked in the range of linear kinetics, but the role of the film as a barrier to oxidation could not be determined. The formation of oxide pustules on martensitic specimens was the only distinct feature indicating a difference in the mode of oxide formation on differently structured alloys. The major product of the reaction at all temperatures irrespective of alloy structure was an oxide whose structure could be indexed as monoclinic zirconia.

Zirconium-niobium alloys containing 2-3 w/o niobium are being utilized in nuclear reactor technology for their desirable mechanical and low neutron absorption properties. A primary disadvantage of poor corrosion resistance for alloys in an appropriate martensitic structure for optimum mechanical behavior has been largely overcome by cold-working and tempering treatments. Dawson (1) has presented a review of the literature on this subject. Although there are many observations on the beneficial effects of tempering on decreasing the corrosion rates of dilute alloys in steam, air, and carbon dioxide atmospheres, studies have not been attempted of structural effects from a fundamental viewpoint. In this investigation, results are reported for the oxidation properties of a Zr-2.7 w/o Nb alloy in both martensitic and Widmanstatten structures exposed to pure oxygen at temperatures in the range 300°-500°C. Alloys of these structures could be readily obtained by vacuum annealing followed by quenching from temperatures in the β solid solution and in the $\beta + \alpha$ phase regions selected from the binary phase diagram (2, 3).

Experimental

The material was a zirconium-2.7 w/o niobium alloy received as 2 mm thick sheet. Analyses for impurities are presented in Table I. Specimens approximately 1 cm² were cut from this sheet and subjected to an appropriate annealing and quenching treatment. Several specimens of the above dimensions were received already in a martensitic structure following a vacuum anneal at 960°C for 10 min before water quenching. They were prepared directly for oxidation tests.

Specimens were prepared by annealing and quenching in an all-metal system capable of maintaining a vacuum of 10^{-6} Torr. In order to minimize contamination from residual gas, specimens were wrapped in

Table I. Analysis of impurity content of Zr-2.7% Nb

Element	ppm (max)	Element	ppm (max)
Al	82	Mo	<10
B	<0.2	N	24
C	100	Ni	50
Cd	<0.3	O	1100
Co	<8	Pb	<5
Cr	30	Si	100
Cu	35	Sn	<100
Fe	980	Ta	<200
H	5	Ti	20
Hf	76	V	<5
Mg	<10	W	<35
Mn	<10	Zn	<50

platinum foil. In all cases, heat-treatments were carried out by raising the furnace already at 1000°C over the annealing tube containing the specimen. The specimen was held at this β-solution temperature of the alloy for 1 hr, and, if the structure required was that of full martensite, it was then quenched into oil. Specimens were also quenched from 800°C, in which cases a specimen was furnace cooled from 1000° to 800°C, held at this temperature for a predetermined time, then quenched into oil.

The surfaces of specimens were prepared by abrasion on SiC papers from 240 through 600 mesh grit under water followed by polishing for several hours on napped cloths, impregnated with 6 and 1μ diamond paste, respectively, and lubricated with kerosene. Final polishing was obtained with a vibratory polisher using a suspension of 0.3μ alumina powder suspended in water. In addition, several specific preparations involving chemical etching and different types of abrasion treatments were employed to determine possible effects of surface preparation on the oxidation kinetics.

Oxidation kinetic experiments were carried out using a vacuum microbalance apparatus (4). These results were supplemented by a series of experiments in which the specimens were intermittently removed for weighing from a quartz reaction tube. Furnaces were controlled to ±2°C, and the oxygen pressure during reaction was 1 atm. Medical grade oxygen was used which was purified by passage through cupric oxide, phosphorous pentoxide, Linde 5Å molecular sieves, and a trap immersed in solid carbon dioxide to remove traces of hydrogen, water vapor, carbon monoxide, and carbon dioxide.

The surfaces of oxidized specimens were examined microscopically and subjected to nickel filtered copper radiation with a recording x-ray diffractometer in order to identify oxide constituents in the scales. Metallographic examinations were carried out on specimen cross sections mounted in bakelite (4). In some instances, it was possible to delineate the structure of two-phase alloys by relief polishing without etching. When an etchant was needed, the most successful was found to be an aqueous solution containing 30 v/o H_2SO_4, 30 v/o HNO_3, and 10 v/o HF at a temperature in the range 68°- 75°C. The volume fraction of proeutectoid α-Zr in a two-phase alloy structure was readily determined by projecting the microstructure on a calibrated objective screen of the microscope at a magnification in the range 200-600X.

Results

In order to determine the reproducibility of measurements and the influence of surface preparation on the reaction rates, several specimens were prepared with different structures and surface preparations for oxidation at 400°C (Fig. 1). Curves (a) and (b) illustrate the oxidation behavior of martensitic specimens subjected to metallographic and chemical polishes. These different preparations did not influence oxidation at long exposures since the rates were of the same magnitude after transition to linear kinetics. In the early stages of the reaction, a correlation was not found between the methods of surface preparation due to the irreproducibility of measurements. However, it was established that the martensitic specimens exhibited oxidation variations dependent upon the heat treatment conditions. This is illustrated by comparing the curves (b), (c), and (d) for specimens quenched into water after vacuum anneals for 10 min at 960° and 1 hr at 1000°C and for the specimen wrapped in platinum foil and quenched into oil after a vacuum anneal of 1 hr at 1000°C, respectively. These oxidation curves are of the same form with the latter specimen exhibiting the slowest rate. This behavior with the platinum-wrapped specimen would be associated with less impurity pickup from the residual gas or the slower rate of cooling during quenching. Martensitic specimens used in this investigation were prepared by both methods and are specified in the results.

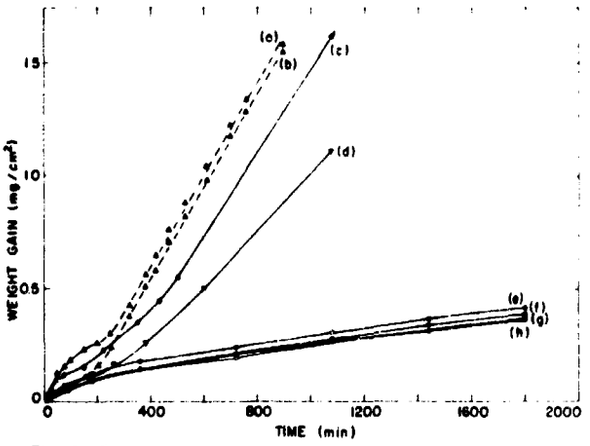

Fig. 1. Oxidation of Zr-2.7 w/o Nb alloy at 400°C in oxygen at 1 atm pressure. (a) anneal 10 min at 960°C, water-quenched, surface chemically polished; (b) anneal 10 min at 960°C, water-quenched, surface metallographically polished; (c) anneal 1 hr at 1000°C, water-quenched, surface metallographically polished; (d) anneal 1 hr at 1000°C, oil-quenched, surface metallographically polished; (e) and (g) anneal 1 hr at 1000°C and 1 hr at 800°C, oil-quenched, surface polished on 0.25μ diamond; (f) and (h) anneal 1 hr at 1000°C and 1 hr at 800°C, oil-quenched, surface polished on 0.3μ alumina.

Possible effects on the oxidation rate due to variations in the final stage of mechanical polishing were also investigated by oxidizing Widmanstatten structured specimens from the same batch heat-treatment (Fig. 1). Curves (e) and (g) were obtained from specimens after a polish with 0.25μ diamond paste on a selvyt cloth, whereas, curves (f) and (h) were obtained from specimens polished on a vibratory pol-

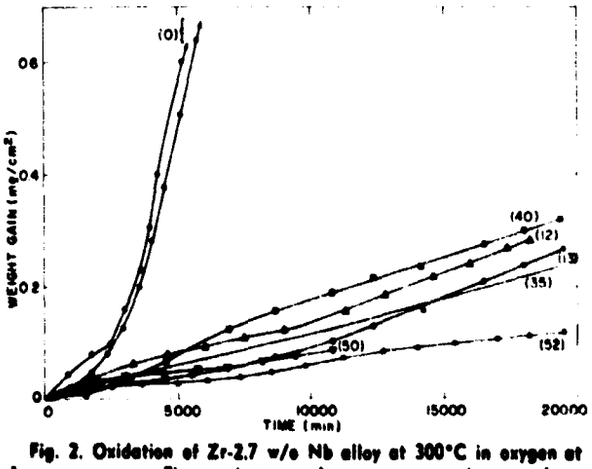

Fig. 2. Oxidation of Zr-2.7 w/o Nb alloy at 300°C in oxygen at 1 atm pressure. Figures in parentheses are approximate volume fractions of α-Zr in the alloys. Martensitic specimens water-quenched.

isher using a suspension of 0.3μ alumina in water. Apparently, the oxidation rate is not influenced by the type of abrasive employed in the final polishing stage.

Typical measurements of oxidation rates at 300°, 400°, and 500°C for various alloys prepared by metallographic polishing are shown in Fig. 2, 3, and 4. Although the kinetics were characterized by a certain degree of irreproducibility in the initial stages, the large variations in the oxidation rates could be correlated with the structures of the specimens. It is apparent from the volume fraction of α-Zr in the alloy listed with each kinetic curve that the oxidation rates at all investigated temperatures decrease with increasing amount of this phase.

Two examples of specimen microstructures obtained by quenching from 800° and oxidized at 400°C are shown in Fig. 5. If the anneal was carried out for only 5 min, structures containing 10-15 v/o α-Zr were obtained. Upon equilibrating an alloy at 800°C, the structure would contain about 50 v/o proeutectoid α-Zr. This condition was found after an anneal for 1 hr. Specimens containing contents of this phase between these two extremes were obtained by annealing within the above time periods.

The topography of an oxidized specimen was dependent on the alloy structure, the reaction temperature, and the time of exposure. A martensitic structured specimen, oxidized at 300° or 400°C, exhibited interference colors to film thicknesses of approximately 2000A with color tints varying from grain to grain. At about the time of transition from an initial decreasing rate to a more rapid approximately linear rate, isolated growths of pustular shape were observed. The densities of these pustules varied with alloy grain orientations (Fig. 6a). These growths spread with lengthening exposure to cover most of the surface, although complete coverage was never observed in the exposure periods of the present experiments (Fig. 6b). On viewing the surface of a pustule at high magnification, fine cracks were observed which appeared to emanate from the tip. These pustules protruding above the main oxide surface only accounted for a relatively small amount of oxide as they were not observed at the surface of metallographic cross sections.

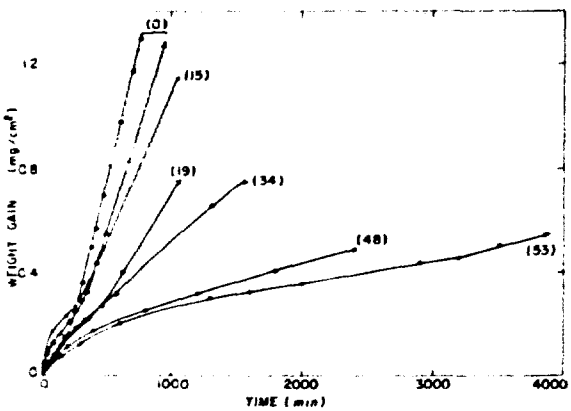

Fig. 3. Oxidation of Zr-2.7 w/o Nb alloy at 400°C in oxygen at 1 atm pressure. Figures in parentheses are approximate volume fractions of α-Zr in the alloys. Martensitic specimens water-quenched.

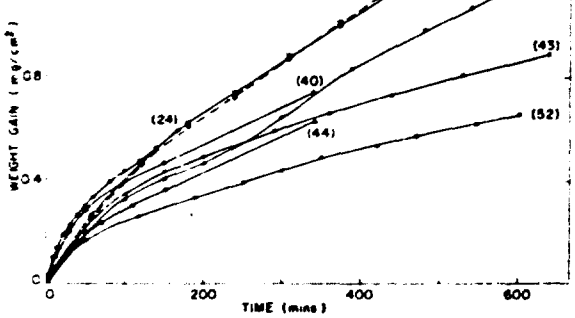

Fig. 4. Oxidation of Zr-2.7 w/o Nb alloy at 500°C in oxygen at 1 atm pressure. Figures in parentheses are approximate volume fractions of α-Zr in the alloys. Martensitic specimens oil-quenched.

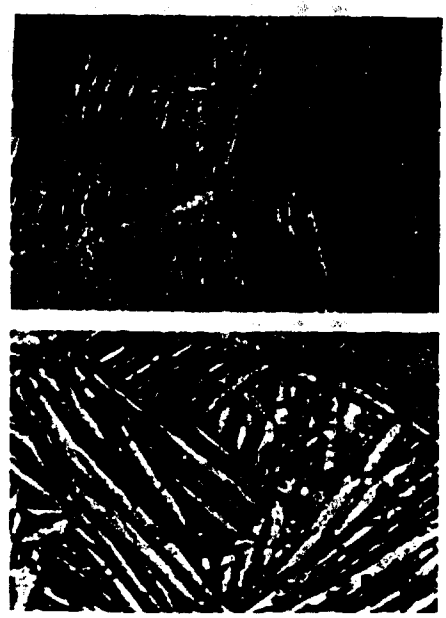

Fig. 5. Microstructures of two specimens quenched from 800° and oxidized at 400°C. a (top), volume fraction of proeutectoid α-Zr ~ 15%; b (bottom), volume fraction of proeutectoid α-Zr ~ 48%.

Martensitic specimens oxidized at 500°C did not exhibit pustules even at brief exposures of 10 min. The oxidized specimens exhibited a gray rippled surface (Fig. 6c). This external appearance indicated that a very large number of small pustules had formed in close proximity without a large degree of lateral growth before their coalescence.

Oxidation of an alloy obtained by quenching from the (α + β) alloy region gave rise to rates of film growth dependen the phase on which the oxide was growing. The growth of oxide on the α-Zr platelets was much less than on the α'-Zr regions. For the conditions and exposures examined, the former film never exhibited other than interference colors. The film on the α' structure gave rise initially to interference colors, but its growth rate was estimated to be at least triple that of the film on α-Zr. The film eventually became gray, and small cracks appeared running parallel to the direction of the α-Zr plates (Fig. 7a). Eventually, these cracks became more extensive and developed into intricate networks (Fig. 7b). Such observations applied to all specimens in this alloy condition, irrespective of the reaction temperature, when reaction had proceeded to linear kinetics. No oxide pustules were observed at any time for this alloy condition by light microscopy.

Cross sections of all oxidized specimens revealed an uneven metal/oxide interface. Martensitic-structured specimens exposed to the transition range for linear kinetics exhibited fine microscopic irregularities

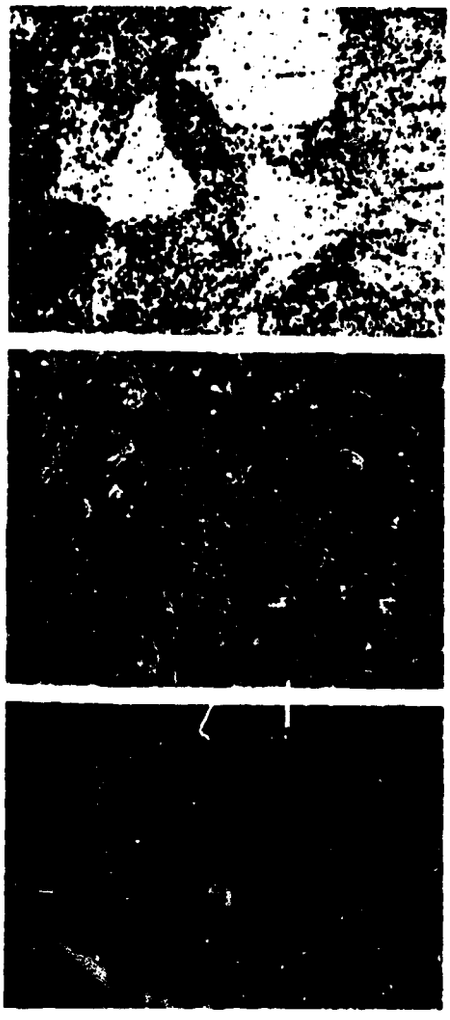

Fig. 6. Topographies of oxidized specimens with martensitic structure. a (top), 400 min at 400°C, oxygen uptake 0.07 mg/cm², magnification 150X; b (center), 1330 min at 400°C, oxygen uptake 1.9 mg/cm², magnification 100X; c (bottom), 300 min at 500°C, oxygen uptake 0.8 mg/cm²; magnification 150X.

and also much larger undulations representing areas, rather than points, of larger oxide penetration (Fig. 8a). At long exposures, the larger variations almost disappeared to leave a relatively uniform thick scale containing cracks, many of which appeared to follow the contour of the metal/oxide interface (Fig. 8b).

The topographical observations on oxidized specimens in the two phase ($\alpha + \alpha' - Zr$) structure were confirmed by the examinations of cross sections (Fig. 9); that is, the rate of oxide growth was greater on the α' structure. This behavior was most vividly illustrated by specimens exposed for long times at 300°C where the oxide formed on the α'-regions had selectively penetrated to the extent that it appeared pinned by the unoxidized α plates (Fig. 9a). This degree of selective penetration became less pronounced with increasing temperature, and the oxide in the external film appeared less cracked at the highest temperature of 500°C (Fig. 9c).

Detailed examination of the metal/oxide interface of all specimens oxidized for relatively long time periods demonstrated that localized points of oxide penetration occurred at the lines of martensitic transformation in the α'-Zr microstructure. This is illustrated by the etched microstructure of the martensitic alloy (Fig. 10a), and by the Widmanstatten-structured alloys (Fig. 9a, 10b) where the fine degree of oxide penetrations into the martensitic structure between the α-Zr plates is readily apparent.

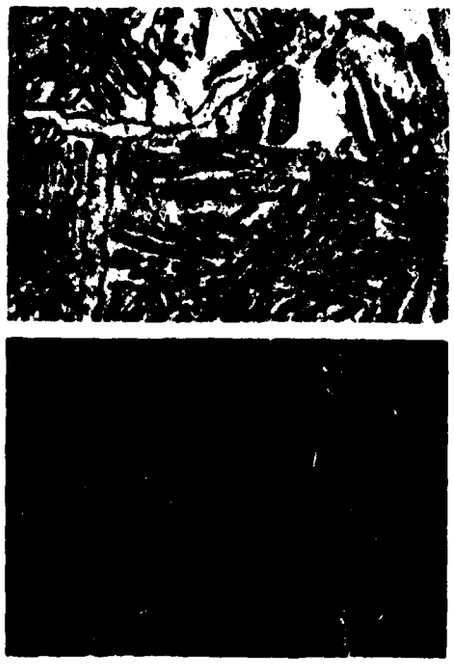

Fig. 7. Topographies of oxidized specimens with Widmanstatten structure. a (top), 10,800 min at 300°C, oxygen uptake 0.09 mg/cm²; magnification ca. 680X; b (bottom), 485 min at 400°C, oxygen uptake 0.5 mg/cm²; magnification ca. 460X.

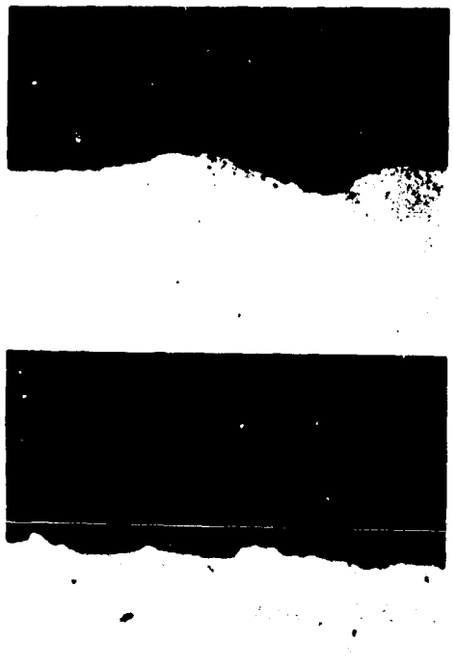

Fig. 8. Cross sections of oxidized specimens with martensitic structures. a (top), 1030 min at 400°C, oxygen uptake 1.1 mg/cm², magnification 675X; b (bottom), 1380 min at 500°C, oxygen uptake 2.0 mg/cm², magnification 675X.

X-ray analyses revealed that the major oxidation product could be indexed as monoclinic zirconia. Occasionally a weak reflection was observed which could be interpreted as either the cubic or tetragonal form of zirconia. Oxides of niobium were not detected. However, the technique is limited and monoclinic zirconia may not be the only reaction product.

Discussion

An attempt has been made to elucidate more fully the oxidation mechanisms of a Zr-Nb alloy by deter-

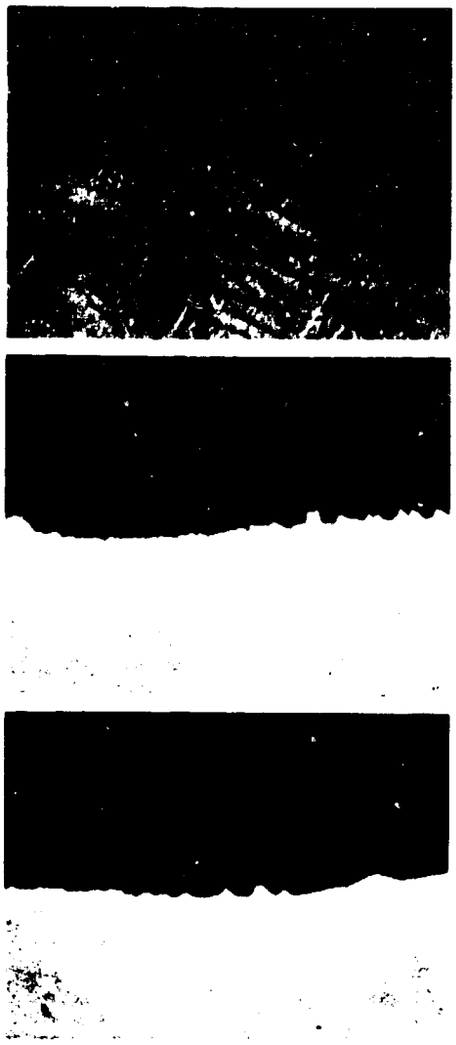

Fig. 9. Cross sections of oxidized specimens with Widmanstatten structures. a (top), 19,300 min at 300°C, oxygen uptake 0.23 mg/cm²; b (center), 485 min at 400°C, oxygen uptake 0.5 mg/cm²; c (bottom), 150 min at 500°C, oxygen uptake 0.5 mg/cm². Magnification 675X.

mining the effects of alloy structures on the oxidation kinetics. The results available at 300° and 400°C (Fig. 2 and 3) gave two limiting oxidation curves for the alloy under examination. A distinct transition was shown in the oxidation curves of the martensitic alloy, prepared by quenching from a β-solid solution temperature. The rate decreased until a transition range was attained in which the rate increased again to a maximum value associated with approximately linear kinetics. The other limiting oxidation curve was shown by alloys with Widmanstatten structures produced by quenching from 800°C and containing approximately 50 v/o proeutectoid α-Zr, the equilibrium amount for this temperature. These curves exhibited a decreasing rate, which, in the later stages, approximated to linear kinetics.

In the early stages of the reaction at 300° and 400°C, there was little difference between the oxidation rates for the two alloy structures. However, the reaction rate at long times of a Widmanstatten-structured alloy was much less than the linear rate of the martensitic alloy. Specimens with intermediate amounts of proeutectoid α-Zr exhibited oxidation rates between these two limiting cases, the over-all rate increasing with decreasing amount of α-Zr.

A direct relationship between the magnitude of the reaction kinetics and the amount of α-Zr in an alloy could not be demonstrated from the present results

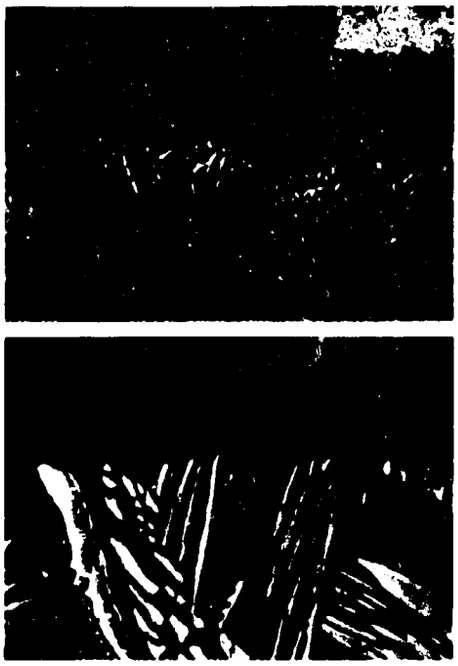

Fig. 10. Etched structures of oxidized specimens. a (top), martensitic structure, 7130 min at 300°C; b (bottom), Widmanstatten structure, 485 min at 400°C. Magnificaion 675X.

at 300° and 400°C. In the initial stages, the oxidation rate of α'-Zr was at least three times faster than α-Zr, while in the final stages of the exposures, the contribution of film growth on the α-Zr plates was of minor significance to the over-all film growth. Moreover, the oxide film on α'-Zr at long exposures was cracked and porous. These observations suggest that the linear oxidation kinetics at 300° and 400°C would be largely dependent on the amount of α'-Zr in the alloy.

Plots of the linear rate constants *vs.* the amount of α'-Zr are shown in Fig. 11 and 12. At 300°C, the kinetic curves were irregular and the rate constants are only approximations. The martensitic specimens reacted rapidly at this temperature, the rate decreasing markedly over the range to 85 v/o martensite. At 400°C, the decrease in rate was proportional to the amount of α'-Zr from full to approximately 80 v/o martensite. A smaller dependence of the oxidation rate on the contents of α'-Zr less than 80 v/o appeared to be associated with the morphological development of the oxide film.

Chemical composition is a major difference between martensite formed by quenching from 1000° and 800°C. α'-Zr formed under the latter condition would contain twice as much niobium. At small niobium contents, alloys with larger niobium concentration exhibit more rapid oxidation (5, 6). Thus, α'-Zr would possibly oxidize more rapidly in the specimens quenched from 800°C. The observations from this investigation do not support this consideration. Accordingly, any variations to be expected from increased niobium concentration in the martensitic phase were suppressed by possible variations in the structure of this phase or its mechanism of oxidation in the presence of proeutectoid α-Zr.

It has been shown that the oxide on the martensitic phase was subject to constraint by α-Zr plates and was pinned beneath the metal/oxide interface, Fig. 9(a). The oxide under such circumstances was less porous and the oxidation rate showed a smaller dependence on the amount of α'-Zr at percentages less than 80 v/o (Fig. 11 and 12). Thus, the over-all oxidation rate became dependent on two factors: the amount of α'-Zr and the penetration depth of oxide into the metal. With low percentages of proeutectoid

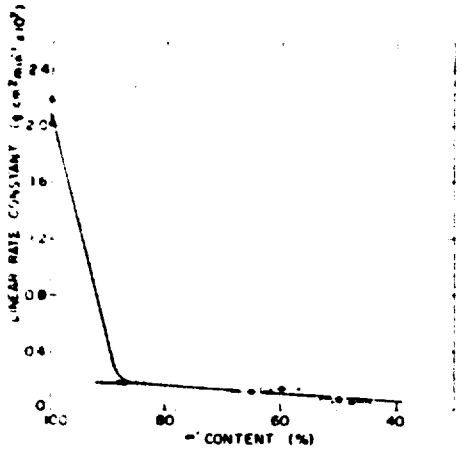

Fig. 11. Plot of linear oxidation rate constants vs. amount of α'-Zr at 300°C.

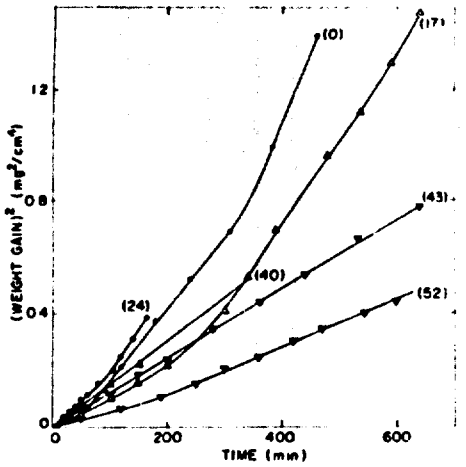

Fig. 13. Oxidation kinetics at 500°C represented by parabolic plots.

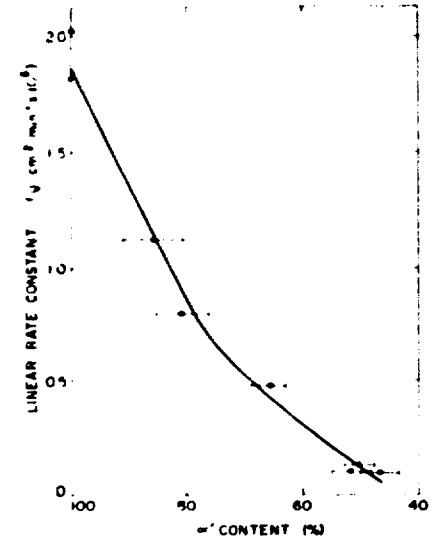

Fig. 12. Plot of linear oxidation rate constants vs. amount of α'-Zr at 400°C.

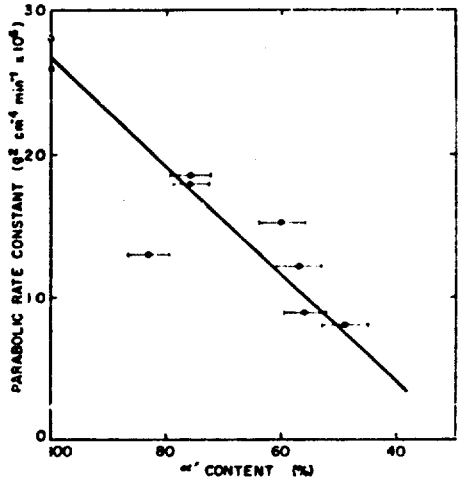

Fig. 14. Plot of parabolic oxidation rate constants vs. amount of α'-Zr at 500°C.

α-Zr, this latter factor was less important, and the over-all rate varied almost linearly with the amount of martensite. However, at large percentages of the proeutectoid phase, oxide on martensite penetrated selectively between plates of the former phase, and the oxidation rate was much slower than to be predicted by a direct proportionality between oxidation rate and amount of α'-Zr.

Oxidation curves at 500°C did not exhibit transitions to more rapid linear kinetics as observed at the two lower temperatures. Although the films on α-Zr were characterized by interference colors, those on the α'-phase were invariably gray at all observed times in contrast to results at the lowest temperatures. Though the oxidation properties were dependent on alloy structure at this highest temperature employed, the kinetics could be represented by parabolic plots for relatively long exposures (Fig. 13). Moreover, a plot of the parabolic constants *vs.* the amount of α'-Zr demonstrated a direct proportionality from full martensite to 50 v/o proeutectoid α-Zr (Fig. 14). This behavior appears reasonable since pronounced selective penetration of oxide between plates of this phase did not occur as at lower temperatures. Tempering of martensite occurs at this temperature and α-Zr would exhibit a larger niobium solubility. The influence of these parameters on oxidation processes in a manner not understood at present may account for the smaller degree of selective phase oxidation.

In view of the fact that the form of the oxidation curve is dependent on both alloy structure and temperature, conclusions drawn from comparisons of results obtained under different exposure conditions must be accepted tentatively. The major product of the reaction of all temperatures, irrespective of alloy structure, was an oxide whose structure could be indexed as monoclinic zirconia. However, it is interesting to compare the differences in surface topography and cross sections of oxidized specimens (Fig. 6-9). At 500°C and while the rate curve was parabolic, the gray oxide which formed did not exhibit cracks distinguishable by light microscopy. The oxidation rate would be possibly controlled by diffusion processes in the oxide film during this stage of the reaction. Cracking of such oxide, however, was noted at 300° and 400°C for all alloys in early periods of exposure at small film thicknesses and parabolic kinetics were not obeyed. On the other hand, the oxide was cracked in the range of approximately linear kinetics at all temperatures, but its role as a barrier to oxidation could not be interpreted by using standard metallographic techniques.

The formation of oxide pustules was the only distinct feature indicating a difference in the mode of oxide formation on different structured alloys. The pustules, moreover, were only observed at the temperatures 300° and 400°C on martensitic specimens and appeared on the surface during the transition to linear kinetics. These specimens were the only ones to exhibit the type of oxidation curve where there was a very pronounced transformation in the kinetics from a small initial rate to a much more rapid rate at long exposures. This behavior, involving pustule formation and cracking, may be associated with interfacial stress between the alloy and the oxide film. At 500°C, such stress might be relieved by tempering of the alloy at the reaction temperature and thus allow a more compact film to form. The presence of the proeutectoid α-Zr plates could similarly aid stress relief and so reduce the possibility of pustule formation, but no substantiating evidence could be found in the present results.

Acknowledgments

The authors were indebted to B. Cox for supplying the Zr-Nb alloy sheets and several specimens in prepared metallurgical structures. This research was completed under auspices of the Atomic Energy of Canada Limited and the Defence Research Board of Canada.

Manuscript received June 2, 1967. This paper was presented at the Chicago Meeting, Oct. 15-19, 1967.

Any discussion of this paper will appear in a Discussion Section to be published in the June 1968 JOURNAL.

REFERENCES

1. J. D. Dawson, U.K.A.E.A. Report AERE-R 4820 (1964).
2. H. Richter, P. Wincierz, K. Anderko, and U. Zeicker, *J. Less Common Metals*, **4**, 252 (1962).
3. G. T. Higgins and E. E. Banks, *Electrochem. Technol.*, **4**, 341 (1966).
4. R. J. Hussey and W. W. Smeltzer, *This Journal*, **111**, 564 (1964).
5. O. Zmeskal and M. L. Brey, *Trans. ASM*, **53**, 415 (1961).
6. R. S. Ambartsumjan, A. A. Kiselev, F. V. Grebenikov, V. A. Myshin, L. J. Tsuprun, and A. F. Nikulina, Proc. 2nd. U.N. Inter. Conf. Peaceful Uses of Atomic Energy, **5**, 12 (1958).

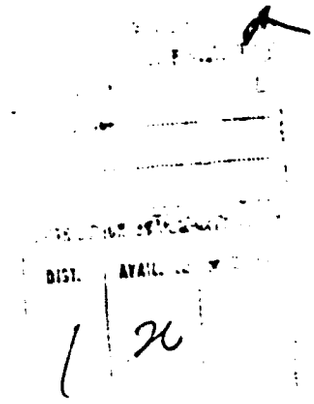

mide. Nuclear magnetic resonance analyses were carried out with a Varian A-60 n.m.r. spectrometer. Analytical gas chromatography was carried out with a F&M Model 300 Gas Chromatograph with 3m, ¼ in. columns packed with 18% Carbowax 20-1% $AgNO_3$ on Chromosorb W, 3% XE-60 on Teflon, 3% Flexol 8N8 on Teflon or silicone grease on Chromosorb W. Vpc analyses were obtained from two or more columns to insure the identity of the peaks.

The dimethylsulfoxide (Matheson, Coleman & Bell) was distilled at reduced pressure from a small amount of sodium hydride, bp 58°-60° (5 mm). The dimethylformamide (DMF) was distilled from barium oxide before use. Styrene (Eastman) was distilled *in vacuo* just before use and stabilized with hydroquinone. Tetra-*n*-butylammonium bromide (Eastman) was recrystallized from ethyl acetate before use. Tetraethylammonium p-toluenesulfonate (Alfred Bader Chemical Company) was recrystallized from acetone.

The electrolytic cell used for macro electrolyses has been described (9). The cathode potential was monitored with a SCE and vacuum tube voltmeter. The power supply was a Nobatron RC150-7.5, and the cell voltage was adjusted so that the cathode potential was near the first wave, half-wave potential of the compound being reduced. The cell voltage was manually controlled later in the run to prevent a large rise in cathode potential. The electrolysis was stopped when the cathode potential would no longer remain near the half-wave potential at a cell current of 0.25 amp indicating that nearly all of the starting material had been consumed. An Analytical Instruments, Inc. current integrator was used to determine the total amount of electricity passed.

The anolyte in each case was a solution of tetraethylammonium p-toluenesulfonate in DMF. Styrene was present in the catholyte in each case to trap reactive intermediates.

Macroelectrolysis of I.—The catholyte consisted of 20.5g (0.075 mole) of cyanomethyldimethylsulfonium p-toluenesulfonate (10), 200 ml of DMF, 30g of tetraethylammonium p-toluenesulfonate and 30 ml of styrene. The electrolysis was carried out at 10°-15°, 1.0-0.25 amp and a cathode voltage of −1.0 to −1.13v (*vs.* SCE). The total quantity of electricity was 0.096F. After the electrolysis, the solvent was removed from the catholyte by distillation at reduced pressure. The strong odor of dimethyl sulfide was present. Vpc analysis of the distillate showed the presence of 2.15g (70% based on starting material) of acetonitrile. The residue after solvent removal was extracted with ether. The residue after removal of the ether from the ether extract contained no 4-phenylbutyronitrile by vpc analysis. Traces of DMF were removed from the residue by distillation at 0.1 mm leaving a black, gummy residue.

A second electrolysis of I was carried out using a glass frit divided H cell with a 20 ml catholyte capacity. The cathode was a 2 cm diameter mercury pool. The anode was platinum foil. The catholyte consisted of 19 ml of 0.915*M* cyanomethyldimethylsulfonium p-toluenesulfonate in dimethylsulfoxide. The anolyte consisted of 27 ml of 1*M* tetra-*n*-butylammonium bromide in dimethylsulfoxide and 1.5 ml of cyclohexene. The catholyte was deaerated with N_2 before the electrolysis and then was sealed. The anolyte was swept with N_2 during the electrolysis. The cathode potential was not monitored. Only a thermometer was in contact with the catholyte. The catholyte was maintained at 20°C during the run by immersing the cell in an ice-water bath. The electrolysis was carried out at 50-60 ma until 8.7 mF of current was passed. After the electrolysis, polarographic analysis of the catholyte and anolyte[a] indicated 1.53 mmoles of I had been consumed. Vpc analysis of the catholyte showed the presence of 3.9 mmoles of acetonitrile (90% yield based on 2 F/mole).[b] No acetonitrile was detected in the anolyte.

Macroelectrolysis of II.—The catholyte was identical to the previous run except that the sulfonium salt (22g, 0.078 mole) was cyanoethyldimethylsulfonium p-toluenesulfonate. The electrolysis was carried out at 0°, 1.0-0.25 amp, and a cathode potential of −1.74 to −1.89v (*vs.* SCE).[c] The total quantity of electricity was 0.097F. The electrolysis was stopped at this point because more than 1F of electricity per mole had been passed, and it was suspected that II had been decomposed[b] to form acrylonitrile, the reduction of which would require 2F/mole. The workup was as described for the previous run and yielded 1.0g (37%) of propionitrile, 0.54g (21.6%) of acrylonitrile and a trace of adiponitrile (all by vpc analysis). No 5-phenylvaleronitrile or mercurials were detected.

A second electrolysis was carried out in a glass frit divided H-cell with a mercury pool cathode and platinum foil anode. The catholyte consisted of 150 ml of dimethylsulfoxide containing 0.1*M* tetra-*n*-butylammonium bromide, 40g (0.14 mole) of dimethylcyanoethylsulfonium p-toluenesulfonate, 30 ml of styrene, and a trace of hydroquinone. The anolyte was dimethylsulfoxide containing 0.1*M* tetra-*n*-butylammonium bromide and saturated with cyclohexene. The cell was maintained at 15° by a water bath. The electrolysis was carried out for 24.25 hr with a cell voltage of 150v, a curernt of 0.2 amp, and at a cathode potential of −1.6v (*vs.* SCE). A total of 0.167F of electricity was passed. The cathode potential did not increase as the 1F/mole of II point was passed, and it was again suspected that decomposition of II had occurred.

After the electrolysis, the catholyte was evacuated to 30 mm through a dry-ice, acetone-cooled trap overnight. The trap overnight collected about 1 ml of a mixture of acrylonitrile, propionitrile, and dimethylsulfide.

Attempts to get a quantitative analysis of acrylonitrile in the catholyte by vpc analysis were futile because II decomposes in the injection port to form acrylonitrile. Attempts to determine the amount of acrylonitrile present in the catholyte by polarography were also unsuccessful because the waves of it and II were too close together.

The catholyte was then mixed with 500 ml of water, and this mixture was extracted with three 200-ml portions of ether. The combined ether extract was back-extracted with water and dried over anhydrous magnesium sulfate. The ether solution was concentrated on a rotary evaporator. The concentrated solution was cooled in dry-ice whereupon 1.2g (5.5%) of biscyanoethylmercury, mp 46°-48° (17), precipitated.

The remainder of the ether was stripped from the solution, and the styrene was removed at reduced pressure (0.9 mm). The residue was distilled at 0.2 mm giving a single cut from 50°-80° (2.0g). Nmr analysis of this indicated 1.0g each of 3-thiomethylpropionitrile (7.1%) and methylcyanoethyl mercury (5.3%). Vpc analysis of the pot residue which contained all the hydroquinone used to prevent styrene polymerization showed the presence of 0.012g of 5-phenylvaleronitrile. (The standard sample of 5-phenylvaleronitrile was obtained from 5-phenylvaleric acid by the usual methods.)

The mixture of 3-methylthiopropionitrile and methylcyanoethyl mercury was redistilled in a micro apparatus. The 3-thiomethylpropionitrile distilled at 50°-60° at 0.2 mm. Two small cuts were then taken at 70° and 71°. The first was used for nmr analysis and

[a] A small amount of I had been forced by hydraulic pressure into the anode compartment.

[b] Due to decomposition of I in the vpc injection port to unknown products which emerge in the dimethyl sulfide region, it was impossible to determine dimethyl sulfide by this method. However nmr analysis of the solution indicated the presence of 7.3 mmoles of dimethyl sulfide in the catholyte (100% loss on 2 F mole). See Discussion.

[c] This electrolysis was carried out at a lower temperature than the others, so that over the duration of the electrolysis (ca. 6 hr) the base catalyzed Hofmann elimination reaction of II could be minimized.

REPRINT NO: 2849 UNCLASSIFIED

PROJECT NO: D44-75-10-39

TITLE: The Oxidation Properties of a Zirconium-2.7 w/o Niobium Alloy in the Temperature Range 300° - 500°C

AUTHORS: M.G. Cowgill and W.W. Smeltzer

DATED: 2 June 1967

SECURITY GRADING: UNCLASSIFIED INITIAL DISTRIBUTION: February 1968

2 - DSIS Circ;

Plus distribution

1 - Ref. File

1 - DREA

1 - DCBRE

1 - CARDE

1 - DREP

1 - DRES

1 - AECL

CANADIAN

3 - CTS
1 - DGOS/TL
1 - DESS
1 - DMES

2 - CDRS(L)
1 - CDLS(L)

1 - WNRE, AECL, Pinawa, Man. Attn: Librarian

MINISTRY OF TECHNOLOGY

1- Periodicals Section

12 - Serial 25
1 - DG of Arty
2 - DSCD Colchester
1 - DGFVE
1 - FVRDE
2 - MFYE
1 - RARDE
2 - AOSR 5
1 - DOAE

1 - RMC of Science

1 - MOD Army (Library)

Continued

MINISTRY OF DEFENCE (ROYAL NAVY)

1 - NSTIC Reports Section
1 - Admiralty Research Lab.
1 - Central Dockyard Lab.
1 - Admiralty Corrosion Committee
1 - Director of Physical Research
1 - Admiralty Materials Lab.

MINISTRY OF DEFENCE (RAF)

1 - Chief Scientist

BRITISH DIRECT

1 - National Physics Lab.
1 - British Standards Institute
1 - Atomic Energy Research Establishment
1 - British Iron & Steel Federation
1 - Interservice Metallurgical Research Council
1 - British Ship Research Association

UNITED STATES

3 - NAVAL ATTACHE, U.S. EMBASSY

26 - SENIOR STANDARDIZATION REP., U.S. ARMY

4 - AIR ATTACHE, US EMBASSY

Plus Suggested Distribution
1 - DDC
1 - NASA